

Prediction of short stellar activity cycles using derived and established empirical relations between activity and rotation periods.

A. k. Althukair^{1,2}  and D. Tsiklauri¹ 

¹ Department of Physics and Astronomy, School of Physical and Chemical Sciences, Queen Mary University of London, Mile End Road, London, E1 4NS, UK; *a.k.althukair@qmul.ac.uk*, *d.tsiklauri@qmul.ac.uk*

² Physics Department, College of Sciences, Princess Nourah Bint Abdulrahman University, Riyadh, PO Box 84428, Saudi Arabia

Received 20xx month day; accepted 20xx month day

Abstract In our previous work, we searched for super-flares on different types of stars, focusing on G-type dwarfs using entire Kepler data to study statistical properties of the occurrence rate of super-flares. The said study also considered how the statistics change with stellar rotation period, which in turn, had to be determined. Using such new data, as a by-product, we found 138 Kepler IDs of F and G types main sequence stars with rotation periods less than a day ($P_{\text{rot}} < 1$ d). On one hand, previous studies have revealed short activity cycles in F-type and G-type stars and the question investigated was whether or not short-term activity cycles are a common phenomenon in these stars. On the other hand, extensive studies exist which establish empirical connection between a star's activity cycle and rotation periods. In this study, we compile all available Kepler data with $P_{\text{rot}} < 1$ d and derive, as well as use plausible, established empirical relations between P_{cyc} and P_{rot} with the aim to provide predictions for very short $5.13 \leq P_{\text{cyc}} \leq 38.14$ d cases in a tabular form. As a result, we invite others to measure P_{cyc} using monitoring program of stellar activity (e.g. activity-related chromospheric emission S-index) or similar means for the Kepler IDs found in this study in order put to test the derived and/or established empirical relations between P_{cyc} and P_{rot} . We also propose an alternative method for measuring very short P_{cyc} , using flare-detection algorithms applied to future space mission data.

Key words: stars: activity — stars: flare — stars: rotation — stars: solar-type — stars:

1 INTRODUCTION

The 11-year cycle of solar activity discovered by Schwabe in 1844 (Schwabe 1844), is a significant phenomenon in solar and stellar physics. The cycle is manifested by a periodic change in solar activity, including the appearance of sunspots and changes in the Sun's magnetic field on this time-scale. Smoothed sunspot numbers have been widely used as a proxy for solar activity over the past four centuries (Shepherd et al. 2014). The idea of the sunspot number was first introduced by Waldmeier (1961) in the mid-19th century, and it has since become a standard measure for quantifying solar activity. These numbers reveal that there are almost regular cycles of about 11 years, reflecting the Sun's magnetic activity.

During the course of a solar cycle, the Sun experiences alternating periods of strong and weak activity known as solar maximum and minimum (Hathaway et al. 2002; Shepherd et al. 2014; Reinhold et al. 2017). As the solar cycle progresses, the magnetic field becomes more complex and twisted. This results in the emergence of sunspots, which are dark areas on the surface of the Sun with intense magnetic fields, vary in size and can last from days to several months (Petrovay & van Driel-Gesztelyi 1997), decaying into bright areas called faculae formed by smaller magnetic concentrations (Reinhold et al. 2017). During the active phase of the solar cycle (solar maximum), the number and size of sunspots increase and appear at the solar surface. At the same time, bright faculae also become more prominent. As the cycle progresses, the number of sunspots decreases, the overall brightness of the Sun remains relatively constant and the Sun enters its least active phase of the solar cycle (solar minimum). These dark and bright features on the Sun's surface contribute to the variability in the total solar irradiance (TSI) (Marchenko et al. 2022). Therefore, the TSI data can capture the combined effects of the evolving dark and bright features during the solar cycle (Domingo et al. 2009; Reinhold et al. 2017).

Cyclic activity has been observed in stars other than the Sun through long-term brightness changes associated with increased occurrence of active regions on their surfaces or in their lower stellar atmospheres Reinhold et al. (2017). The Mount Wilson HK program, which started in 1966 and lasted until the end of the 20th century, was the first to conduct a systematic search for activity cycles in main sequence stars (Wilson 1978; Baliunas et al. 1995; Mittag et al. 2019a). By analysing chromospheric emission in the spectral lines of Ca II H&K, as the magnetic field connected to active regions on the surfaces of stars plays an important role in transporting energy into the chromosphere. This increased energy input into the chromosphere leads to enhanced chromospheric emission, which can be observed prominently in the cores of the Ca II H&K spectral lines Reinhold et al. (2017). The measure of the chromospheric emission strength is described by the Mount Wilson S-index (Vaughan et al. 1978) or by the quantity R'_{HK} (Brandenburg et al. 2017). Vaughan & Preston (1980) investigated the chromospheric activity levels in main-sequence F-G-K-M stars by measuring the chromospheric CaII H&K emission fluxes. They noted that these stars display varying degrees of chromospheric activity and observed a noticeable lack in the number of F-G stars displaying intermediate activity compared to both highly active and less active stars. They suggested that the absence of such stars could be attributed to a decline in chromospheric activity as the stars age. Noyes et al. (1984a) examined the relationship between chromospheric activity, specifically the R'_{HK} activity index, and the Rossby number $\text{Ro} = P_{\text{rot}}/\tau_c$ for a sample of main-sequence stars of spectral type F or later. Where P_{rot}

a strong correlation between the R'_{HK} activity index and the Rossby number. However, in contrast to the findings of Vaughan & Preston (1980), Noyes et al. (1984a) did not find any signs of the “Vaughan-Preston gap”. Noyes et al. (1984b) investigated the empirical relation between rotation period P_{rot} , spectral type, and activity cycle period P_{cyc} for 13 slowly rotating main-sequence stars. They found that the cycle period is related to the rotation period by a power law: $P_{\text{cyc}} \propto P_{\text{rot}}^{1.25}$. This relationship can alternatively be expressed as $P_{\text{cyc}} \approx \text{Ro}^{1.25} \approx (P_{\text{rot}}/\tau_c)^{1.25}$ (Brandenburg et al. 2017; Mittag et al. 2023). For stars of spectral type G0-K5, Baliunas et al. (1995) observed a pattern of variation in the rotation period and the measure of chromospheric activity (S-index). Their research revealed that the chromospheric activity levels were high in young stars with fast rotation periods. Chromospheric activity and rotation rates of stars in the intermediate age range were average. Alternatively, the chromospheric activity levels were low in old stars with slow rotation periods. This observation supports the existence of the Vaughan-Preston gap (Reinhold et al. 2017), indicating that chromospheric activity and rotation change over time as the stars age. The relation between rotation periods and activity cycles of a sample of stars was investigated by Baliunas et al. (1996), who discovered a correlation between the two variables. In particular, they observed that stars with slower rotation periods exhibit longer activity cycles, while stars with faster rotation periods tend to have shorter activity cycles. According to Oláh & Strassmeier (2002), the relation between rotation periods and cycle lengths is more evident for stars with shorter activity cycles. However, the association becomes less clear for longer cycle lengths when considering more recent findings on the time variability of solar cycles.

Vida et al. (2013) investigated the behaviour and activity cycles of four fast-rotating late-type stars with ($P_{\text{rot}} \leq 0.5$ days), highlighting the presence of 1-year cycles and the correlation between rotation rate and cycle length. Vida et al. (2014) used the short-term Fourier transform, a time-frequency analysis method, to examine the light curves of 39 fast-rotating late-type active stars with rotation periods of less than one day. Nine of the selected stars showed indications of activity cycles with periods between 300 and 900 days. These cycles were inferred from the changing typical latitude of the starspots on the stellar surface and due to the differential rotation of the stellar surface, the observed rotation period of the stars varied over the activity cycle. This variation in the rotation period was attributed to the movement and evolution of starspots at different latitudes of the star. Reinhold et al. (2017) used four years of Kepler data to determine the cyclic variations in the amplitude of the light curve and the rotation period of stars by analysing a sample of active stars and calculating the rotation period and variability amplitude for each star in each Kepler quarter. Then they searched for periodic variations in these time series using Lomb-Scargle periodograms and employed a false alarm probability (FAP) criterion for selection. The study’s findings indicate that amplitude periodicities, associated with underlying activity cycles, are detected in 3203 stars with cycle periods ranging from 0.5 to 6 years and rotation periods ranging from 1 to 40 days. According to Brandenburg et al. (2017) analysis of new observations and previous data, the longer and shorter cycle periods closely match expectations based on the average activity levels and rotation periods, which indicates a connection between stellar activity and stellar rotation. Baliunas et al. (1995) reported an activity cycle of 11.6 years in the F-type star τ Boo (HD 120136). However, the authors assigned a FAP “poor” grade to this finding. Mittag et al. (2017b) detected an activity cycle with a duration of 122 days

exhibit variations on a relatively short timescale. Mittag et al. (2019a) focused on exploring the presence of short-term activity cycles in F-type stars, specifically using S-index time series data obtained with the TIGRE telescope. They utilized the generalized Lomb-Scargle periodogram method to analyze the data and search for periodic variations with a maximum length of 2 years. Their sample of F-type stars identified four stars that exhibited cyclic variations with periods of less than a year. However, compared to solar-type stars with well-developed cyclic activity, the amplitude of these short-term cyclic variations in F-type stars was smaller. Based on their findings, Mittag et al. (2019a) concluded that the activity behaviour among F-type stars differs from that of the Sun and cooler main sequence stars. By studying 44 main-sequence stars with confirmed activity cycles, and rotation periods, Mittag et al. (2023) examined the relation between the length of the activity cycle and the Rossby number (Ro). They used empirical turnover periods based on the B-V colour index to calculate Rossby numbers, from which they deduced an empirical relationship between the Rossby number and the cycle duration. The study showed linear behaviour in the double-logarithmic relationship between the Rossby number and cycle period. In addition, the relative convection zone depth was found to be correlated with cycle length and convective turnover time.

In paper I (Althukair & Tsiklauri 2023a), we looked for super-flares on different types of stars and focused on G-type dwarfs using entire Kepler data to study various aspects of statistical properties of the occurrence rate of super-flares. In paper II (Althukair & Tsiklauri 2023b), as a by-product, we found thirteen peculiar Kepler IDs that are Sun-like, slowly rotating with rotation periods of 24.5 to 44 days, and yet can produce a super-flare and six G-type and four M-type Kepler IDs with exceptionally large amplitude super-flares. As noted previously, these detections defy our current understanding of stars and hence deserve a further investigation. In this paper III, the last in this series, we use an empirical connection between a star's activity cycle and rotation periods for a sample of F and G main sequence stars with rotation periods of less than one day. Here our aim is to provide predictions for very short activity cycle cases in a tabular form and to investigate in the future whether these short activity cycles are a common phenomenon in these stars or not. Section 3.3 provides the target selection method. Section 3 presents the method used in this work which includes the empirical connection relation between P_{cyc} and P_{rot} . The main findings of the study are presented in Section 4, and section 5 concludes this work with our main conclusions.

2 RELATION BETWEEN ACTIVITY CYCLE AND ROTATION PERIOD

Parker (1955) model of the α - Ω dynamo introduced the concept of migratory dynamo waves, which play a crucial role in generating the observed solar cycle (Mittag et al. 2023). The α -effect, arising from the twisting of rising magnetic field tubes due to Coriolis forces, creates the poloidal magnetic field required for the next sunspot cycle. This effect is responsible for the reversal of magnetic polarities between successive cycles (Parker 1955; Mittag et al. 2023). On the other hand, the Ω -effect, resulting from the differential rotation of the star, generates a toroidal magnetic field by stretching the magnetic field lines in a longitudinal direction. The combination of the α -effect and the Ω -effect leads to the formation of migratory dynamo waves, where the toroidal field is periodically regenerated and transformed into the poloidal field through the action of the α -effect. These migratory dynamo waves propagate and interact within the star's convective

According to Noyes et al. (1984b), the magnetic cycle period for G and K dwarfs with convective turnover times (τ_c) between 11 and 26 days, is found to be proportional to the rotation period as follows:

$$1/P_{\text{cyc}} \propto (\tau_c/P_{\text{rot}})^n, \quad (1)$$

where n is 1.25. We quote theoretical prediction of the relation between star's activity cycle and its rotation periods, which is equation (6) in Mittag et al. (2023):

$$P_{\text{mag.cyc}} = 2P_{\text{cyc}} \approx \sqrt{\frac{R_\star}{l}} P_{\text{rot}}. \quad (2)$$

According to the simple theoretical arguments quoted by Mittag et al. (2023), the magnetic cycle period $P_{\text{mag.cyc}}$ is proportional to the rotation period P_{rot} . However, there is a modifying factor, l/R_\star the relative depth of turbulence, which depends on the stellar structure, which itself may depend on the effective temperature or B-V colour index of the star. Also l here is the length scale of turbulence and R_\star is the stellar radius.

3 METHODS

In our study, we adopt the terminology used by Brandenburg et al. (2017); Mittag et al. (2023) to categorize branches into two types: the "inactive" branch, referred to as the short-cycle branch P_{cyc}^S and the "active" branch, referred to as the long-cycle branch P_{cyc}^L . These terms were introduced first time in Brandenburg et al. (2017). According to Mittag et al. (2023) this notation is more accurate and aligned with the actual characteristics of the branches. Therefore, they suggested that these terms should be used in future studies to refer to the two branches.

3.1 Reproduction of Mittag et al. (2023) P_{cyc}^S vs. P_{rot} Fit

In this subsection, we reproduced the fit between P_{cyc}^S and P_{rot} data from Mittag et al. (2023) to derive the fit parameters. First, we collected the data in Table 1, the first 32 rows, from Mittag et al. (2023), where we obtained the 32 activity cycles on the short-cycle branch P_{cyc}^S calculated by Mittag et al. (2023) along with the 32 corresponding rotation periods P_{rot} . These cycle lengths and rotation periods can be found in Table 1. Then we plotted in logarithmic scale the rotation periods on the x-axis versus the calculated cycle period on the y-axis as shown in Figure 1, using the empirical relation in Mittag et al. (2023) between the cycle periods and rotation periods in logarithmic terms that is given by:

$$\log P_{\text{cyc}} \approx a + n \log P_{\text{rot}}. \quad (3)$$

Since the theoretical relation, equation 2 implies a linear connection between P_{cyc} and P_{rot} , we fitted the data using Python *least-square* fit, a common technique for determining the best-fitting parameters for a given model, for two different slope adjustments as in Mittag et al. (2023). Also, we computed the R^2 coefficient of determination to measure how well the model fits the data. A R^2 value of 1 means that the predictions from the regression fit the data perfectly. First, we set the slope n to be 1 and deduced the value of a parameter as $a = 1.923 \pm 0.025$ and the value of $R^2 = 0.89$. The red line in Figure 1 illustrates this

equation now 3 becomes:

$$\log P_{\text{cyc}} \approx (1.458 \pm 0.074) + (1.348 \pm 0.054) \log P_{\text{rot}}. \quad (4)$$

and the value of $R^2 = 0.95$. The blue line in Figure 1 represents this fit. It is obvious that the $n = 1$ relation does not fit the short periods data, as Mittag et al. (2023) pointed out.

By comparing the value of a and n parameters here with Mittag et al. (2023), we find slight differences between these values. As in Mittag et al. (2023) $a = 1.918 \pm 0.027$ for the fit of $n=1$, while for the fit where n is treated as a free parameter, $a = 1.488 \pm 0.092$ and $n = 1.324 \pm 0.067$. We noticed two additional points in Figure 1 of Mittag et al. (2023), which belong to stars HD 100563 and HD 201092. These stars have rotation periods of 7.73 ± 0.04 and 37.8 ± 7.4 , respectively, corresponding to cycle lengths of 0.609 ± 0.009 and 11.7 ± 0.4 , respectively. Their P_{cyc} were taken from Mittag et al. (2019a) and Brandenburg et al. (2017), respectively, and have not been calculated by Mittag et al. (2023). We do not have these two points because our plot include only data computed by Mittag et al. (2023). We also noticed that the locations of some points in our plot differ from those in Mittag et al. (2023) plot, despite using the same data set. We believe these reasons led to the slight difference in the fit parameters between this work and Mittag et al. (2023).

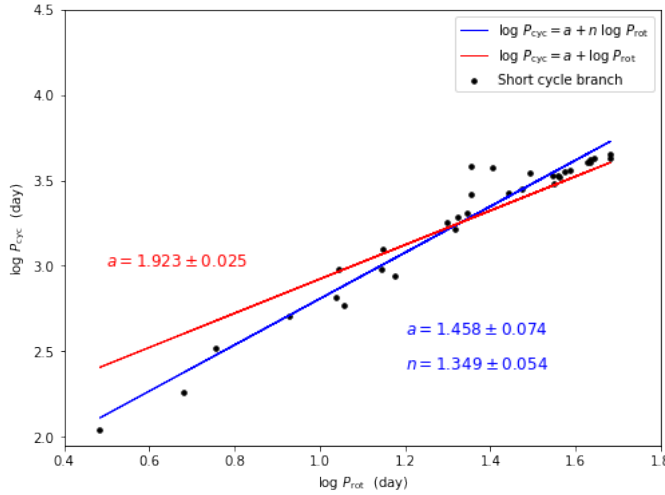


Fig. 1: Log-scale of rotation period versus log-scale of cycle period (short cycle branch) for a sample of stars taken from Mittag et al. (2023). The deduced fit of P_{rot} vs. P_{cyc} relation are shown as solid lines. The blue line shows the fit when slope n is treated as an independent parameter while the red line shows the fit with a fixed slope of $n=1$.

3.2 Data representation and fit

In this subsection, we repeat the fit between P_{rot} and P_{cyc}^S using a larger data sample taken from other previous studies. This sample, shown in Table 1, contains 94 P_{rot} and their 94 corresponding P_{cyc}^S . The star ID, spectral type (Sp), color index (B-V), effective temperature (T_{eff}), P_{rot} and P_{cyc} are shown in Table 1. Unavailable data is left blank in the table. 32 P_{cyc}^S were calculated by Mittag et al. (2023), the first 32 lines

et al. (2022); Egeland et al. (2015); Flores et al. (2016); Ferreira et al. (2020); Ferreira Lopes et al. (2015); Moutou et al. (2016); Mittag et al. (2017b, 2019a,b); Olsper et al. (2018); Salabert et al. (2016). It should be noted that the 32 stars IDs for which their P_{cyc}^S were calculated by Mittag et al. (2023) were used again in the fit but with the P_{cyc}^S calculated by others. For illustration, we used two P_{cyc}^S values for 32 stars IDs, one was calculated by Mittag et al. (2023) and the other was calculated by another work, except for KIC 10644253, for which we collected three P_{cyc}^S calculated by Salabert et al. (2016); Brandenburg et al. (2017); Mittag et al. (2023). Also, HD 16673 has multiple entries due to the multiple sources, as shown in Table 1. References for each P_{rot} and P_{cyc}^S are shown in Table 1.

In the same way as in subsection 3.1, we used the empirical relation between P_{rot} and P_{cyc} in logarithmic scale given by equation 3 using the new data set in Table 1 to produce the fit parameters a and n . We performed a *least-square* fit in Python to fit the data using two different slope adjustments again, one with a fixed slope n of 1 and another with the n treated as a free variable. This fit is shown in Figure 2. For the fit with a fixed slope of 1, we determined the value for the parameter $a = 1.889 \pm 0.023$ and $R^2 = 0.83$. This trend is shown by the red line in Figure 2. While for the fit with the slope n treated as a free variable, we deduced values for the parameters a and n as $a = 1.583 \pm 0.064$, $n = 1.257 \pm 0.051$ and $R^2 = 0.87$. This fit is represented by the blue line in Figure 2. So that equation 3 becomes now

$$\log P_{\text{cyc}} \approx (1.583 \pm 0.064) + (1.257 \pm 0.051) \log P_{\text{rot}}. \quad (5)$$

We note that our value of $n = 1.257 \pm 0.051$ with the extended dataset is closer to Noyes et al. (1984b)'s $n = 1.25$ than Mittag et al. (2023)'s $n = 1.324 \pm 0.067$.

Table 1: list of star IDs with their parameters, used in previous studies.

HD/KIC	T_{eff}	B-V	τ_c	$P_{\text{rot}}[\text{d}]$	Ref	$P_{\text{cyc}}^S[\text{yr}]$	Ref
Sun	5777	0.642	33.94	25.4 ± 1	1	10.3	15
HD 3651	5211	0.850	61.18	44	1	11.7	15
HD 4628	5120	0.890	65.19	38.5 ± 2.1	1	9.9	15
HD 10476	5244	0.836	59.83	35.2 ± 1.6	1	9.2	15
HD 10780	5321	0.804	56.87	22.14 ± 0.55	2	5.6	15
HD 16160	5060	0.918	68.16	48 ± 4.7	1	12.4	15
HD 16673	6183	0.524	18.02	5.7	3	0.9	15
HD 17051	6045	0.561	21.98	8.5 ± 0.1	1	1.4	15
HD 22049	5140	0.881	64.27	11.1 ± 0.1	1	2.6	15
HD 26965	5282	0.820	58.33	43	1	11.5	15
HD 30495	5804	0.632	32.16	11.4 ± 0.2	1	1.6	15
HD 32147	4801	1.049	83.93	48	1	11.7	15
HD 43587	5876	0.610	28.58	22.6 ± 1.9	4	10.4	15
HD 75332	6089	0.549	20.60	4.8	5	0.5	15
HD 75732	5167	0.869	63.05	37.4 ± 0.5	6	9.7	15

Continued on next page

Table 1 – continued from previous page

HD/KIC	T_{eff}	B-V	τ_c	$P_{\text{rot}}[\text{d}]$	Ref	$P_{\text{cyc}}^S[\text{yr}]$	Ref
HD 76151	5714	0.661	37.58	15	1	2.4	15
HD 100180	6013	0.570	23.06	14	1	3.4	15
HD 103095	5449	0.754	52.52	31	1	9.6	15
HD 120136	6245	0.508	16.54	3.05±0.01	7	0.3	15
HD 128621	5098	0.900	66.24	36.2±1.4	1	9.2	15
HD 140538	5645	0.684	42.51	20.71±0.32	8	4.5	15
HD 146233	5741	0.652	35.81	22.7±0.5	1	7.2	15
HD 149661	5265	0.827	58.98	21.1±1.4	1	5.3	15
HD 160346	4975	0.959	72.75	36.4±1.2	1	9	15
HD 165341 A	5188	0.860	62.16	19.9	1	4.9	15
HD 166620	5151	0.876	63.76	42.4±3.7	1	11.1	15
HD 185144	5366	0.786	55.26	27.7±0.77	2	7.3	15
HD 190406	5910	0.600	27.09	13.9±1.5	1	2.6	15
HD 201091	4764	1.069	86.64	35.4±9.2	1	8.3	15
HD 219834 B	5055	0.920	68.38	43	1	11	15
KIC 8006161	5234	0.840	60.21	29.8±3.1	1	7.7	15
KIC 10644253	5943	0.590	25.67	10.9±0.9	1	1.8	15
HD 16673	6183	0.524	18.02	7.4±0.07	5	0.85	5
HD 49933				3.45	5	0.58	5
HD 75332	6089	0.549	20.60	4.8	5	0.49	5
HD 100563				7.73	5	0.61	5
τ Boo		0.480	14.23	3.5	5	0.33	5
Kepler 87				12.59±0.03	9	3.5	16
KIC 10644253	6030	0.590	25.67	10.91±0.87	10	1.5	17
solar analog HD 30495	5826	0.632	32.16	11.36±0.17	11	1.67±0.35	11
solar analog HD 45184	5871	0.620	30.16	19.98±0.02	12	5.14	12
61 Cyg A HD 201091	4545	1.069	86.64	35.7±1.9	13	7.2±1.3	13
102712791		0.277	4.79	0.96±0.03	14	0.09±0.008	14
102720703		0.514	17.08	10.2±0.6	14	0.512±0.055	14
102721955		0.431	10.94	2.17±0.06	14	1.118±0.071	14
102723038		1.404	147.52	8.6±0.5	14	1.682±0.151	14
102726103		0.767	53.62	3.7±0.1	14	0.321±0.022	14
102738457		0.592	25.95	12.9±0.6	14	1.781±0.356	14
102749950		0.657	36.78	5.4±0.2	14	0.655±0.06	14
102750723		1.143	97.45	1.44±0.02	14	0.277±0.022	14
102754736		0.480	14.23	6.9±0.3	14	0.29±0.019	14

Continued on next page

Table 1 – continued from previous page

HD/KIC	T_{eff}	B-V	τ_c	$P_{\text{rot}}[\text{d}]$	Ref	$P_{\text{cyc}}^S[\text{yr}]$	Ref
102758108		0.641	33.75	6.1 ± 0.2	14	0.301 ± 0.022	14
102770332		2.055	415.00	4.2 ± 0.1	14	1.162 ± 0.112	14
102770893		0.874	63.56	4.3 ± 0.2	14	0.759 ± 0.058	14
102777006		1.177	102.86	1.33 ± 0.02	14	1.17 ± 0.123	14
102778595		1.157	99.64	11.8 ± 0.7	14	0.575 ± 0.019	14
102780281		1.304	125.85	3 ± 0.1	14	0.551 ± 0.041	14
Sun	5778	0.660	37.38	25.4 ± 1	1	11 ± 2	1
HD 3651	5128	0.840	60.21	44	1	13.8 ± 0.4	1
HD 4628	5035	0.890	65.19	38.5 ± 2.1	1	8.6 ± 0.1	1
HD 10476	5188	0.840	60.21	35.2 ± 1.6	1	9.6 ± 0.1	1
HD 16160	4819	0.980	75.21	48 ± 4.7	1	13.2 ± 0.2	1
HD 17051	6053	0.570	23.06	8.5 ± 0.1	1	1.6	1
HD 22049	5152	0.880	64.17	11.1 ± 0.1	1	2.9 ± 0.1	1
HD 26965	5284	0.820	58.33	43	1	10.1 ± 0.1	1
HD 30495	5780	0.630	31.82	11.4 ± 0.2	1	1.7 ± 0.3	1
HD 32147	4745	1.060	85.41	48	1	11.1 ± 0.2	1
HD 76151	5675	0.670	39.44	15	1	2.5 ± 0.1	1
HD 78366	5915	0.630	31.82	9.7 ± 0.6	1	5.9 ± 0.1	1
HD 81809	5623	0.800	56.51	40.2 ± 3	1	8.2 ± 0.1	1
HD 100180	5942	0.570	23.06	14	1	3.6 ± 0.1	1
HD 103095	5035	0.750	52.19	31	1	7.3 ± 0.1	1
HD 114710	5970	0.580	24.33	12.3 ± 1.1	1	9.6 ± 0.3	1
HD 128620	5809	0.710	48.98	22.5 ± 5.9	1	19.2 ± 0.7	1
HD 128621	5230	0.880	64.17	36.2 ± 1.4	1	8.1 ± 0.2	1
HD 146233	5767	0.650	35.42	22.7 ± 0.5	1	7.1	1
HD 149661	5199	0.800	56.51	21.1 ± 1.4	1	4 ± 0.1	1
HD 160346	4797	0.960	72.86	36.4 ± 1.2	1	7 ± 0.1	1
HD 166620	5000	0.900	66.24	42.4 ± 3.7	1	15.8 ± 0.3	1
HD 190406	5847	0.610	28.58	13.9 ± 1.5	1	2.6 ± 0.1	1
HD 201091	4400	1.180	103.35	35.4 ± 9.2	1	7.3 ± 0.1	1
HD 201092	4040	1.370	139.77	37.8 ± 7.4	1	11.7 ± 0.4	1
KIC 8006161	5488	0.840	60.21	29.8 ± 3.1	1	7.4 ± 1.2	1
KIC 10644253	6045	0.590	25.67	10.9 ± 0.9	1	1.5 ± 0.1	1
HD 165341 A	5023	0.780	54.74	19.9	1	5.1 ± 0.1	1
HD 219834 A	5461	0.800	56.51	42	1	21 ± 1	1
HD 219834 B	5136	0.910	67.30	43	1	10 ± 0.2	1

Continued on next page

Table 1 – continued from previous page

HD/KIC	T_{eff}	B-V	τ_c	$P_{\text{rot}}[\text{d}]$	Ref	$P_{\text{cyc}}^S[\text{yr}]$	Ref
HD 10780	5321	0.804	56.87	22.14 ± 0.55	2	7.53 ± 0.16	2
HD 16673	6183	0.524	18.02	5.7	3	0.847 ± 0.006	5
HD 43587	5876	0.610	28.58	22.6 ± 1.9	4	10.44 ± 3.03	4
HD 75732	5167	0.869	63.05	37.4 ± 0.5	6	10.9	18
HD 185144	5366	0.786	55.26	27.7 ± 0.77	2	6.66 ± 0.05	2
HD 120136	6245	0.508	16.54	3.05 ± 0.01	7	0.333 ± 0.002	7
HD 140538	5645	0.684	42.51	20.71 ± 0.32	8	3.88 ± 0.02	8

Notes: The table illustrates a list of stars ID with their corresponding B–V values, effective temperature T_{eff} , the convective turnover time τ_c which was calculated by the relation in Mittag et al. (2018), the rotation period P_{rot} with the reference number and the short branch cycle period P_{cyc}^S with the reference number.

References: (1) Brandenburg et al. (2017), (2) Olsper et al. (2018), (3) Noyes et al. (1984b), (4) Ferreira et al. (2020), (5) Mittag et al. (2019a), (6) Mittag et al. (2017a), (7) Mittag et al. (2017b), (8) Mittag et al. (2019b), (9) McQuillan et al. (2014), (10) García et al. (2014), (11) Egeland et al. (2015), (12) Flores et al. (2016), (13) Boro Saikia et al. (2016), (14) Ferreira Lopes et al. (2015), (15) Mittag et al. (2023), (16) Moutou et al. (2016), (17) Salabert et al. (2016), (18) Baum et al. (2022).

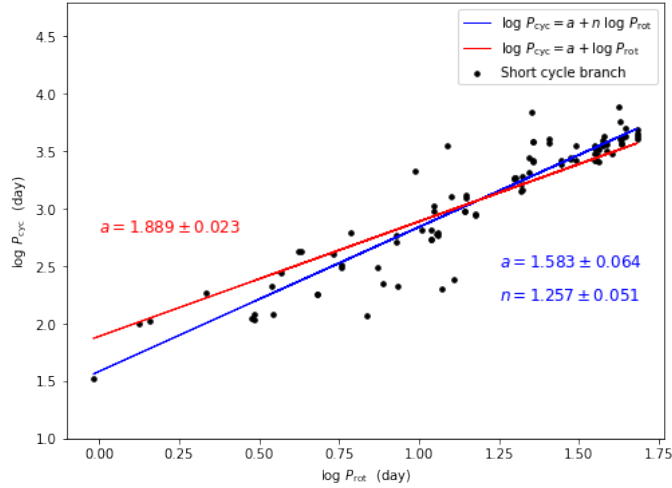


Fig. 2: Log-scale of rotation period versus log-scale of cycle period (short cycle branch) for a 94 samples of stars taken from previous studies in Table 1. The deduced fit of P_{rot} vs. P_{cyc} relation are shown as solid lines. The blue line shows the fit where slope n is treated as an independent parameter while the red line shows the fit with a fixed slope of $n=1$.

3.3 Data Samples

One of the main challenges in studying the relation between cycle length and rotation period is the lack number of well-known and accurately measured activity cycles. This limitation introduces uncertainties in the derived empirical relations Mittag et al. (2023). To overcome these challenges, it is crucial to obtain more reliable cycle periods, particularly for long-period cycles. Achieving this requires long-term time

(2023). Therefore, when looking for activity cycles, it is more efficient to monitor fast-rotating objects, as cycles can be discovered within a few years of observation, as opposed to stars with longer rotation periods Vida et al. (2013). For this reason, we chose our sample for this study to include fast-rotating main-sequence stars of type F and G from Kepler data with well-known rotation periods of less than one day. First, we collected all Kepler IDs which has well-known rotation periods. We then selected targets with rotation periods of less than a day. Using *Gaia* Data Release 2 (*Gaia*-DR2), we identified F- and G-type main sequence stars by their effective temperatures and radius based on the Harvard Spectral classification. The ranges of the effective temperature are 6000-7500 K and 5200-6000 K for F and G types, respectively. We thus obtained a total of 811 Kepler IDs of F- and G- type stars with less than one day rotation period. By using the radius restriction of the main-sequence stars as $1.15\text{-}1.4 R_{\odot}$ and $0.96\text{-}1.15 R_{\odot}$ for F and G types, respectively, the final data sample reduced to 138 Kepler targets with a number of 83 F-type and 55 G-type main-sequence stars. 71.74% of the rotation periods for these stars were taken from McQuillan et al. (2014). 15.94% from Santos et al. (2021), 5.07% from Reinhold & Gizon (2015), 4.35% from Chowdhury et al. (2018) and 2.90% from Yang & Liu (2019). These 138 Kepler targets are listed in Table 2 with their effective temperature, radius, rotation period and the references for these rotation periods.

4 RESULTS

Using a data set of 138 Kepler IDs with P_{rot} ranging from 0.202 d to 0.997 d, we provide a prediction for the corresponding value of their P_{cyc}^S , by applying the empirical relation between P_{cyc} and P_{rot} with the derived parameters in Equation 5. Hence we obtained the predicted values of P_{cyc} from

$$P_{\text{cyc}} \approx 10^{(1.583 \pm 0.064) + (1.257 \pm 0.051) \log P_{\text{rot}}}. \quad (6)$$

From equation 6, we calculated 138 P_{cyc} for 83 F-type and 55 G-type main-sequence stars whose rotation period is less than a day. The shortest P_{cyc} is equal to 5.13 d while the longest P_{cyc} is equal to 38.14 d. All the 138 predicted P_{cyc} are listed in Table 2

Table 2: lists of the 138 Kepler IDs with their parameters and predicted P_{cyc} .

KIC	T_{eff}	R_{\odot}	$P_{\text{rot}}[\text{d}]$	Ref	$P_{\text{cyc}}[\text{d}]$	KIC	T_{eff}	R_{\odot}	$P_{\text{rot}}[\text{d}]$	Ref	$P_{\text{cyc}}[\text{d}]$
757099	5521	1.05	0.36	1	10.60	6877871	6508	1.40	0.54	2	17.73
1028018	5544	1.14	0.62	2	21.03	6948098	6095	1.29	0.57	3	18.76
1721795	6534	1.31	0.89	2	32.93	6961285	5802	0.98	0.45	2	13.99
1872192	5316	0.98	0.67	2	23.31	6962901	5601	0.97	0.98	2	37.37
2557335	5568	1.01	0.24	2	6.20	7199002	6381	1.24	0.57	2	18.89
2558273	6673	1.35	0.99	2	37.85	7199013	5286	0.96	0.57	2	18.89
2715228	6374	1.30	0.99	1	37.80	7199037	6024	1.36	0.57	2	18.89
2715410	5997	1.11	0.90	1	33.53	7354297	5481	1.05	0.95	2	35.99
2849645	5424	1.06	1.00	2	38.14	7461022	6168	1.28	0.59	2	19.76
2985825	6783	1.23	0.94	3	35.18	7678509	6644	1.22	0.96	2	36.51

Continued on next page

Table 2 – continued from previous page

KIC	T_{eff}	R_{\odot}	$P_{\text{rot}}[\text{d}]$	Ref	$P_{\text{cyc}}[\text{d}]$	KIC	T_{eff}	R_{\odot}	$P_{\text{rot}}[\text{d}]$	Ref	$P_{\text{cyc}}[\text{d}]$
3124412	6302	1.21	0.93	1	34.94	7707736	5644	1.09	0.76	2	27.11
3241517	6283	1.34	0.78	3	28.19	7816211	6050	1.32	0.29	2	8.08
3352959	6476	1.37	0.76	2	27.07	7909399	6574	1.40	0.82	2	30.01
3356577	6746	1.39	0.63	4	21.58	7915824	6231	1.39	0.74	2	26.22
3448722	5872	1.13	0.41	2	12.60	7973882	5512	1.06	0.35	2	10.27
3448817	6792	1.33	0.95	4	35.78	8016369	6734	1.34	0.77	1	27.56
3459311	5789	1.05	0.98	2	37.37	8043256	6680	1.27	0.93	2	34.71
3550386	6006	1.30	0.32	2	9.10	8144578	6639	1.32	0.59	2	19.85
3836772	6210	1.32	0.69	2	23.88	8197275	5604	1.14	0.44	2	13.52
3869099	5607	1.01	0.29	2	7.94	8264155	6738	1.33	0.91	4	34.08
4175618	5369	1.05	0.41	2	12.60	8264659	5417	1.12	0.97	1	36.84
4283120	6202	1.25	0.52	2	16.71	8285970	5639	1.14	0.57	2	18.72
4374659	5824	1.03	0.23	2	5.87	8313378	6624	1.31	0.54	2	17.73
4386947	5681	1.14	0.65	2	22.10	8382253	5695	1.01	0.63	3	21.37
4464528	6392	1.38	0.22	2	5.81	8393626	5893	1.15	0.43	2	13.06
4464530	6545	1.30	0.22	2	5.77	8420730	5770	1.08	0.25	2	6.53
4570231	5661	0.99	0.54	1	17.64	8651921	6473	1.29	0.95	2	35.65
4660562	5677	0.96	0.77	1	27.56	8687209	5650	1.00	0.77	1	27.56
4762130	6202	1.35	0.80	2	28.78	8804962	6586	1.23	0.90	2	33.53
4774370	6546	1.36	0.93	2	34.85	8892124	5263	1.01	0.72	2	25.38
4816098	6239	1.29	0.95	1	35.89	8916436	6566	1.35	0.87	1	32.13
4850965	5503	1.04	0.61	2	20.40	9146690	5387	1.11	0.72	2	25.20
4949214	6511	1.36	0.92	2	34.52	9206726	6876	1.31	0.46	4	14.61
4949350	6587	1.40	0.88	2	32.37	9306290	5571	1.04	0.82	2	29.97
4949766	6587	1.39	0.81	2	29.19	9393015	5877	1.01	0.24	2	6.40
5038288	5785	0.99	0.88	2	32.51	9456932	5875	0.97	0.53	2	17.24
5107198	6077	1.36	0.36	2	10.67	9474101	5945	1.10	0.21	2	5.32
5273178	6774	1.32	0.88	2	32.65	9594038	6694	1.31	0.94	4	35.56
5397765	6251	1.34	0.94	2	35.47	9640204	6620	1.33	0.53	2	17.32
5426665	6323	1.38	0.39	2	11.80	9640472	6076	1.34	0.34	2	9.68
5444276	6475	1.31	0.71	2	24.71	9710612	5867	1.08	0.39	2	11.80
5450307	6398	1.24	0.99	3	37.85	9730249	6479	1.34	0.91	2	33.77
5480545	6535	1.31	0.93	2	35.09	9896552	6279	1.26	0.87	1	32.13
5514866	5487	0.97	0.28	2	7.66	9897710	5840	1.08	0.43	2	13.21
5514871	5220	1.06	0.28	2	7.66	9965888	5589	1.13	0.31	2	8.82
5543840	6518	1.20	0.82	2	29.69	9970838	6429	1.25	0.96	2	36.42

Continued on next page

Table 2 – continued from previous page

KIC	T_{eff}	R_{\odot}	$P_{\text{rot}}[\text{d}]$	Ref	$P_{\text{cyc}}[\text{d}]$	KIC	T_{eff}	R_{\odot}	$P_{\text{rot}}[\text{d}]$	Ref	$P_{\text{cyc}}[\text{d}]$
5623538	6729	1.32	0.99	1	37.80	10023062	6469	1.38	0.89	2	33.11
5623852	5886	1.10	0.57	2	18.89	10134084	5926	1.00	0.55	5	18.06
5629449	6897	1.31	0.71	1	24.89	10490282	5504	1.05	0.79	2	28.42
5646176	6302	1.20	0.99	1	37.80	10614890	5283	1.06	1.00	2	38.14
5795235	6517	1.36	0.91	2	34.00	10809099	6051	1.31	0.91	2	33.91
5898014	6697	1.35	0.83	2	30.20	11017401	5648	1.09	0.80	2	28.96
5988566	6299	1.20	0.44	2	13.52	11018874	6454	1.30	0.99	2	37.99
6114118	6234	1.24	0.94	2	35.32	11247377	6184	1.38	0.40	2	12.02
6114140	6384	1.16	0.93	3	35.13	11349677	6076	1.23	0.84	1	30.75
6145032	6315	1.28	0.81	1	29.37	11400413	6781	1.34	0.76	4	27.27
6149358	6660	1.28	0.89	2	32.93	11498689	5464	1.10	0.31	2	8.78
6219870	5663	1.05	0.81	1	29.37	11653059	6160	1.26	0.29	2	8.08
6224148	6230	1.18	0.20	2	5.13	11924842	5494	1.13	0.84	5	30.75
6385867	5306	1.06	0.58	1	19.30	11969131	6444	1.23	0.63	1	21.42
6386598	6658	1.37	0.76	2	27.20	12067121	6211	1.33	0.43	5	13.25
6391602	5782	0.99	0.42	2	12.83	12108612	5695	1.09	0.71	2	24.76
6421219	6191	1.36	0.79	2	28.51	12119534	5296	0.98	0.64	2	21.97
6449077	6366	1.31	0.94	2	35.51	12121738	6134	1.31	0.73	2	25.73
6529902	6604	1.38	0.29	2	8.08	12157161	6513	1.26	0.78	2	27.79
6693864	6846	1.35	0.86	1	31.67	12157799	6117	1.17	0.89	5	33.07
6836589	5628	1.15	0.73	2	25.91	12354328	5251	0.97	0.81	2	29.33
6846595	6718	1.26	0.99	1	37.80	12356839	5605	1.14	0.35	2	10.05
6854461	6547	1.39	0.95	3	36.03	12418959	6427	1.36	0.78	2	28.10

Notes: Effective temperature T_{eff} and radius R_{\odot} was taken from (*Gaia*-DR2).

References: (1) Santos et al. (2021), (2) McQuillan et al. (2014), (3) Reinhold & Gizon (2015), (4) Chowdhury et al. (2018), (5) Yang & Liu (2019).

After predicting the values of the activity cycles for our extended, compared to Mittag et al. (2023), data sample, we wish to examine the theoretical prediction given by Equation 2 on short $P_{\text{cyc}} < 1$ yr. This is because the latter equation is a theoretical prediction, based on first physical principles, as opposed to empirical fit, which lacks any theoretical or conceptual justification. Therefore, we focused on the activity cycles derived from previous studies, as presented in Table 1. We chose 20 stars whose P_{cyc} is less than a year and plot the fit between P_{rot} and P_{cyc} as shown in Figure 3 using a simple linear regression without an intercept given by

$$P_{\text{cyc}} [\text{yr}] = n P_{\text{rot}} [\text{d}]. \quad (7)$$

We obtained the slope $n = 0.081 \pm 0.009$ and R^2 value is 0.997, which is an indication of a good fit, despite

for the lower and upper bounds of our 138 Kepler IDs with P_{rot} ranging from 0.202 d to 0.997 d, this simple theoretically justified equation predicts for $P_{\text{cyc}} = 0.081 \times 0.202 \times 365.25 = 5.98$ d and $0.081 \times 0.997 \times 365.25 = 29.50$ d, which are not very different from applying the more accurate powerlaw fit using equation 6 of 5.13 d and 38.14 d, respectively.

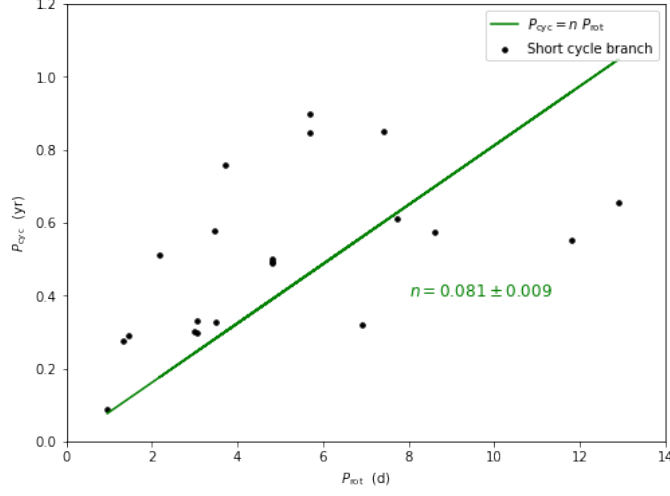


Fig. 3: P_{rot} vs. P_{cyc} using a simple linear regression without an intercept for a sample of stars whose P_{cyc} is less than 1 year. The determined fit of P_{rot} vs. P_{cyc} relation are shown as a solid green line.

Finally, we examine the convective turnover time, τ_c , vs. $B - V$ colour index appearance as in Figure 3 from Mittag et al. (2023). In general, direct measurements of convective turnover time are not possible. However, its estimation is possible by analysing stars' rotation and activity data. As pointed out by Jao et al. (2022), scaling the rotation periods with with a colour- or mass-dependent τ_c can reduce scatter in the relation between rotation and activity, leading to a broken power-law fit between activity and the Rossby number, as e.g. in Mittag et al. (2018). Pizzolato et al. (2001) present a comprehensive study of the convective turnover time, τ_c , and its dependence on stellar metallicity and age of main-sequence stars with masses between $0.6 - 1.6 M_{\odot}$ and they also remark that there is a substantial variation between the different models, as e.g. Stepien (1994) using chromospheric and coronal data, obtained a significantly flatter curve for $B - V > 0.8$ than widely-used Noyes et al. (1984a), see figure 4 from Pizzolato et al. (2001). We plot convective turnover time, τ_c , vs. $B - V$ colour index in figure 4. Figure 4 used the following expressions for the dependence of the convective turnover time τ_c on the $B - V$ color index, as derived from Mittag et al. (2018):

$$\log \tau_c = (1.06 \pm 0.07) + (2.33 \pm 0.37)((B - V) - 0.44) \quad (8)$$

for $0.44 \leq B - V \leq 0.71$. In the case when $B - V > 0.71$ then

$$\log \tau_c = (1.69 \pm 0.12) + (0.69 \pm 0.13)((B - V) - 0.71). \quad (9)$$

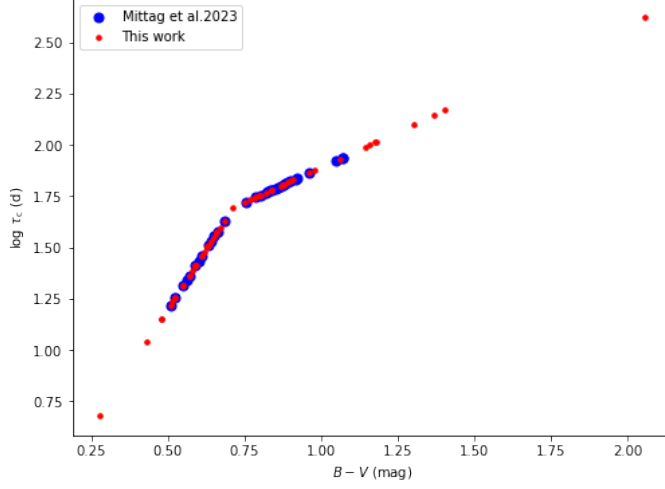


Fig. 4: convective turnover time, τ_c , vs. $B - V$ colour index. Blue dots correspond to Mittag et al. (2023), while red ones are from this study.

5 CONCLUSIONS

In this work, we studied the empirical relation between star activity cycle and rotation period. First, we reproduced the fit between P_{rot} and P_{cyc} using Mittag et al. (2023) data and obtained the following fit parameters $\log P_{\text{cyc}} \approx (1.458 \pm 0.074) + (1.348 \pm 0.054) \log P_{\text{rot}}$, which are slightly different from the Mittag et al. (2023)'s $a = 1.488 \pm 0.092$ and $n = 1.324 \pm 0.067$, for the reasons unknown to us. Then, using a larger data set made up of 94 P_{rot} and their 94 associated P_{cyc} taken from prior studies, we again re-examined the fit between P_{rot} and P_{cyc} and obtained the following fit parameters $\log P_{\text{cyc}} \approx (1.583 \pm 0.064) + (1.257 \pm 0.051) \log P_{\text{rot}}$. Using these new parameters, we applied this relation to a sample of 83 F-type and 55 G-type main sequence stars whose rotation periods of less than one day. To provide tabular predictions for cases with very short activity cycles, in order to determine in the future whether or not these short activity cycles are a common occurrence in these stars. As a result we derived 138 predicted P_{cyc} ranging from 5.13 d to 38.14 d, which are listed in Table 2.

Usefulness of measuring short stellar activity cycles hinges on two main general difficulties:

(i) If monitoring program of stellar activity (e.g. activity-related chromospheric emission S-index or similar) is used as in references such as Mittag et al. (2019a); or Baum et al. (2022), then cadence time of observations is too long e.g. according to table 2 from the latter reference cadence could be 87 observations per year i.e. $365/87 = 4$ days. Resolving activity cycles with $5.13 \leq P_{\text{cyc}} \leq 38.14$ d with such cadence would be nearly impossible.

(ii) If Kepler data light curves are used for e.g. plotting number of flares per day vs. time then large number of flare-detection would be necessary to have a reliable statistics. However, the problem is long cadence, 30 minutes, for the mainstream Kepler data. The photometer used by Kepler is sensitive to wavelengths ranging from 400 to 865 nm, covering the entire visible spectrum and a fraction of the infrared. The accuracy of the photometer of Kepler is approximately 0.01% or 0.1 mmag, when 30-minute integration times are used while considering stars with a magnitude of 12. Kepler's 30-minute integration detected flare

ranged from one to three hours, with a rapid increase followed by a slow, exponential decline Maehara et al. (2012). When Kepler data is taken at a higher cadence or sampling rate of one minute, the accuracy of the measurements decreases. However, this higher cadence enables Kepler to detect flares that are too brief to be detected reliably using the main 30-minute integrations. With the one-minute cadence, Kepler can detect flares with energies as low as 10^{32} ergs Maehara et al. (2015).

It is worth noting that earlier studies exist using different observations where the energy involved in the observed transient brightening is estimated to range from 10^{25} to 10^{29} erg Shimizu (1995). Also, as far as the Sun is concerned, studies exist Mason et al. (2023) which consider flare frequency as a function of flare energy in the range 10^{27} to 10^{31} erg, but this is applicable to the Sun only.

In order to have a good statistics for Kepler IDs considered, we need to detect flares with energies 10^{27-32} ergs in order to see variation number of flares per day on a time scale of $5.13 \leq P_{cyc} \leq 38.14$ d. To achieve this goal a new space mission is necessary with short time cadence (< 1 minutes) and photometric accuracy $< 0.01\%$. A typical example of such proposed sample data from the space mission is shown in figure 5. Alternative option could be making more short cadence ground-based s-index monitoring program

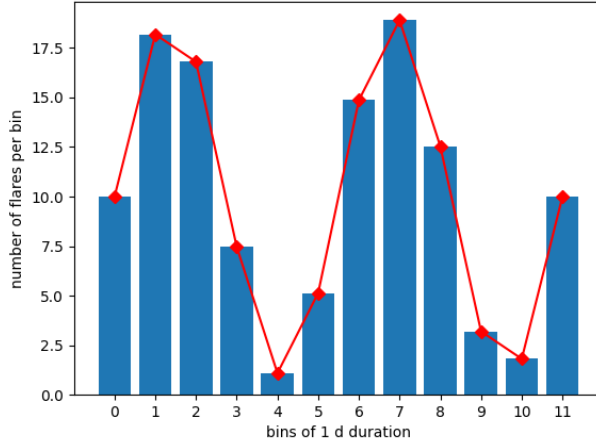


Fig. 5: A sketch of typical data from the hypothetical space mission which will typically measure, say, 10 flares per day, on average, in a bin of 1 d duration. y-axis shows number of flares per bin observed and x-axis shows a bin numer. Bin heights show number of flares detected in that bin, while red line shows the stellar activity cycle temporal trend.

of stellar activity with cadence ≈ 1 d or less. However it is unclear whether this is technically feasible. In any case, the present study provides predictions for $5.13 \leq P_{cyc} \leq 38.14$ d and we hope that future either space or ground-based observational missions will put to test our predictions. Until such time the jury is still out.

ACKNOWLEDGEMENTS

Some of the data presented in this paper were obtained from the Mikulski Archive for Space Telescopes (MAST). STScI is operated by the Association of Universities for Research in Astronomy, Inc., under

Space Science via grant NNX13AC07G and by other grants and contracts.

Authors would like to thank Deborah Kenny of STScI for kind assistance in obtaining the data, Cozmin Timis and Alex Owen of Queen Mary University of London for the assistance in data handling at the Astronomy Unit.

A. K. Althukair wishes to thank Princess Nourah Bint Abdulrahman University, Riyadh, Saudi Arabia and Royal Embassy of Saudi Arabia Cultural Bureau in London, UK for the financial support of her PhD scholarship, held at Queen Mary University of London.

DATA AVAILABILITY

Some of the data underlying this article were accessed from Mikulski Archive for Space Telescopes (MAST) <https://mast.stsci.edu/portal/Mashup/Clients/Mast/Portal.html>. This paper also has made use of data from the European Space Agency (ESA) mission *Gaia* (<https://www.cosmos.esa.int/gaia>), processed by the *Gaia* Data Processing and Analysis Consortium (DPAC, <https://www.cosmos.esa.int/web/gaia/dpac/consortium>). Funding for the DPAC has been provided by national institutions, in particular the institutions participating in the *Gaia* Multilateral Agreement. The derived data generated in this research will be shared on reasonable request to the corresponding author.

References

- Althukair, A. K., & Tsiklauri, D. 2023a, RAA, doi: 10.1088/1674-4527/acdc09
- . 2023b, RAA (minor revision in progress), doi: 10.48550/arXiv.2306.02292
- Baliunas, S. L., Nesme-Ribes, E., Sokoloff, D., & Soon, W. H. 1996, *ApJ*, 460, 848, doi: 10.1086/177014
- Baliunas, S. L., Donahue, R. A., Soon, W. H., et al. 1995, *ApJ*, 438, 269, doi: 10.1086/175072
- Baum, A. C., Wright, J. T., Luhn, J. K., & Isaacson, H. 2022, *AJ*, 163, 183, doi: 10.3847/1538-3881/ac5683
- Boro Saikia, S., Jeffers, S. V., Morin, J., et al. 2016, *A&A*, 594, A29, doi: 10.1051/0004-6361/201628262
- Brandenburg, A., Mathur, S., & Metcalfe, T. S. 2017, *ApJ*, 845, 79, doi: 10.3847/1538-4357/aa7cfa
- Chowdhury, S., Joshi, S., Engelbrecht, C. A., et al. 2018, *Ap&SS*, 363, 260, doi: 10.1007/s10509-018-3480-1
- Domingo, V., Ermolli, I., Fox, P., et al. 2009, *Space Sci. Rev.*, 145, 337, doi: 10.1007/s11214-009-9562-1
- Egeland, R., Metcalfe, T. S., Hall, J. C., & Henry, G. W. 2015, *ApJ*, 812, 12, doi: 10.1088/0004-637X/812/1/12
- Ferreira, R. R., Barbosa, R., Castro, M., et al. 2020, *A&A*, 640, A46, doi: 10.1051/0004-6361/201937219
- Ferreira Lopes, C. E., Leão, I. C., de Freitas, D. B., et al. 2015, *A&A*, 583, A134, doi: 10.1051/

- Flores, M., González, J. F., Jaque Arancibia, M., Buccino, A., & Saffe, C. 2016, *A&A*, 589, A135, doi: 10.1051/0004-6361/201628145
- García, R. A., Ceillier, T., Salabert, D., et al. 2014, *A&A*, 572, A34, doi: 10.1051/0004-6361/201423888
- Hathaway, D. H., Wilson, R. M., & Reichmann, E. J. 2002, *Sol. Phys.*, 211, 357, doi: 10.1023/A:1022425402664
- Jao, W.-C., Couperus, A. A., Vrijmoet, E. H., Wright, N. J., & Henry, T. J. 2022, *The Astrophysical Journal*, 940, 145, doi: 10.3847/1538-4357/ac9cd8
- Kepler Mission. 2019, *Kepler Stellar Properties Table*, IPAC, doi: 10.26133/NEA6
- Maehara, H., Shibayama, T., Notsu, Y., et al. 2015, *Earth, Planets and Space*, 67, 59, doi: 10.1186/s40623-015-0217-z
- Maehara, H., Shibayama, T., Notsu, S., et al. 2012, *Nature*, 485, 478, doi: 10.1038/nature11063
- Marchenko, S. V., Lean, J. L., & DeLand, M. T. 2022, *ApJ*, 936, 158, doi: 10.3847/1538-4357/ac8a98
- Mason, J. P., Werth, A., West, C. G., et al. 2023, *ApJ*, 948, 71, doi: 10.3847/1538-4357/accc89
- McQuillan, A., Mazeh, T., & Aigrain, S. 2014, *ApJS*, 211, 24, doi: 10.1088/0067-0049/211/2/24
- Mittag, M., Hempelmann, A., Schmitt, J. H. M. M., et al. 2017a, *A&A*, 607, A87, doi: 10.1051/0004-6361/201630262
- Mittag, M., Robrade, J., Schmitt, J. H. M. M., et al. 2017b, *A&A*, 600, A119, doi: 10.1051/0004-6361/201629156
- Mittag, M., Schmitt, J. H. M. M., Hempelmann, A., & Schröder, K. P. 2019a, *A&A*, 621, A136, doi: 10.1051/0004-6361/201834319
- Mittag, M., Schmitt, J. H. M. M., Metcalfe, T. S., Hempelmann, A., & Schröder, K. P. 2019b, *A&A*, 628, A107, doi: 10.1051/0004-6361/201935654
- Mittag, M., Schmitt, J. H. M. M., & Schröder, K. P. 2018, *A&A*, 618, A48, doi: 10.1051/0004-6361/201833498
- . 2023, *arXiv e-prints*, arXiv:2306.05866, doi: 10.48550/arXiv.2306.05866
- Moutou, C., Donati, J. F., Lin, D., Laine, R. O., & Hatzes, A. 2016, *MNRAS*, 459, 1993, doi: 10.1093/mnras/stw809
- Noyes, R. W., Hartmann, L. W., Baliunas, S. L., Duncan, D. K., & Vaughan, A. H. 1984a, *ApJ*, 279, 763, doi: 10.1086/161945
- Noyes, R. W., Weiss, N. O., & Vaughan, A. H. 1984b, *ApJ*, 287, 769, doi: 10.1086/162735
- Oláh, K., & Strassmeier, K. G. 2002, *Astronomische Nachrichten*, 323, 361, doi: 10.1002/1521-3994(200208)323:3/4<361::AID-ASNA361>3.0.CO;2-1
- Olsper, N., Lehtinen, J. J., Käpylä, M. J., Pelt, J., & Grigorievskiy, A. 2018, *A&A*, 619, A6, doi: 10.1051/0004-6361/201732525
- Parker, E. N. 1955, *ApJ*, 122, 293, doi: 10.1086/146087
- Petrovay, K., & van Driel-Gesztelyi, L. 1997, *Sol. Phys.*, 176, 249, doi: 10.1023/A:1004988123265

- Pizzolato, N., Ventura, P., D'Antona, F., et al. 2001, *A&A*, 373, 597, doi: 10.1051/0004-6361:20010626
- Reinhold, T., Cameron, R. H., & Gizon, L. 2017, *A&A*, 603, A52, doi: 10.1051/0004-6361/201730599
- Reinhold, T., & Gizon, L. 2015, *A&A*, 583, A65, doi: 10.1051/0004-6361/201526216
- Salabert, D., Régulo, C., García, R. A., et al. 2016, *A&A*, 589, A118, doi: 10.1051/0004-6361/201527978
- Santos, A. R. G., Breton, S. N., Mathur, S., & García, R. A. 2021, *ApJS*, 255, 17, doi: 10.3847/1538-4365/ac033f
- Schwabe, H. 1844, *Astronomische Nachrichten*, 21, 233
- Shepherd, S. J., Zharkov, S. I., & Zharkova, V. V. 2014, *ApJ*, 795, 46, doi: 10.1088/0004-637X/795/1/46
- Shimizu, T. 1995, *PASJ*, 47, 251
- Stepien, K. 1994, *A&A*, 292, 191
- STScI. 2016, Kepler LC, Q0-Q17, STScI/MAST, doi: 10.17909/T9488N
- Vaughan, A. H., & Preston, G. W. 1980, *PASP*, 92, 385, doi: 10.1086/130683
- Vaughan, A. H., Preston, G. W., & Wilson, O. C. 1978, *PASP*, 90, 267, doi: 10.1086/130324
- Vida, K., Kriskovics, L., & Oláh, K. 2013, *Astronomische Nachrichten*, 334, 972, doi: 10.1002/asna.201211973
- Vida, K., Oláh, K., & Szabó, R. 2014, *MNRAS*, 441, 2744, doi: 10.1093/mnras/stu760
- Waldmeier, M. 1961, *The sunspot-activity in the years 1610-1960* (Zurich: Schulthess)
- Wilson, O. C. 1978, *ApJ*, 226, 379, doi: 10.1086/156618
- Yang, H., & Liu, J. 2019, *ApJS*, 241, 29, doi: 10.3847/1538-4365/ab0d28